Title: A load-bearing function for the cytoplasmic membrane of *Escherichia coli*

Authors: Jiawei Sun[1], Miriam Min-Chen Cheng[1], Ellen van Wijngaarden[2], Christopher J. Hernandez[3], Thomas G. Bernhardt[4,5], Kerwyn Casey Huang[1,6,7,†]

Affiliations:

[1]Department of Bioengineering, Stanford University, Stanford, CA 94305, USA

[2]Sibley School of Mechanical and Aerospace Engineering, Cornell University, Ithaca, NY 14850, USA

[3]Departments of Orthopaedic Surgery and Bioengineering and Therapeutic Sciences, UCSF

[4]Department of Microbiology, Harvard University Medical School, Boston, MA 02115, USA

[5]Howard Hughes Medical Institute, Harvard University Medical School, Boston, MA 02115, USA

[6]Department of Microbiology and Immunology, Stanford University School of Medicine, Stanford, CA 94305, USA

[7]Chan Zuckerberg Biohub, San Francisco, CA 94158, USA

21 †To whom correspondence should be addressed: kchuang@stanford.edu

22

23 Keywords: MreB; cytoplasmic membrane; cell wall; peptidoglycan; mechanical

24 coupling; osmotic shocks; membrane stiffness; elongasome; transglycosylase;

25 MltG

Abstract

The structural integrity of bacterial cells is traditionally attributed to the peptidoglycan cell wall, and more recently to the outer membrane, with the cytoplasmic membrane assumed to be mechanically passive. Cells lacking filaments of the actin homolog MreB are more bendable, suggesting a role for the cytoskeleton in cell stiffness. Here, we show that MreB does not stiffen the envelope directly, but instead mechanically couples the cell wall to the cytoplasmic membrane through its role in peptidoglycan synthesis, increasing resistance to bending. Under hyperosmotic stress, MreB relocalized to the poles, forming linkages that prevent membrane detachment from the cell wall and attenuate cytoplasmic contraction. Disruption of MreB filament formation, nutrient starvation, or inactivation of glycan elongation factors abolished or reduced this coupling, revealing that peptidoglycan biosynthesis actively mediates stress distribution across surface layers. Our findings redefine the bacterial envelope as a mechanically integrated composite, with the cytoplasmic membrane having substantial load-bearing capacity.

42 **Introduction**

43 The bacterial cell envelope is a versatile and dynamic structure that acts as a
44 chemical barrier and supports cell growth and division. The envelope bears
45 mechanical stresses from both inside the cell and the external environment[1],
46 including forces due to fluid flow, solid substrates, and osmolarity changes[2]. In
47 particular, a major function of the envelope is to withstand the turgor pressure
48 generated by high solute concentrations in the cytoplasm[3,4]. In Gram-negative
49 bacteria, the envelope consists of a peptidoglycan cell wall sandwiched by the
50 cytoplasmic and outer membranes. The outer membrane is an asymmetric
51 bilayer with phospholipids in the inner leaflet and lipopolysaccharides in the
52 outer leaflet that have important roles in chemical permeability[5]. The cell wall is
53 a rigid macromolecule that has well-recognized importance as an antibiotic
54 target[6] and in resisting cell expansion due to turgor pressure[7]. Robust envelope
55 growth and division requires coordination by a host of enzymes[8]. In many rod-
56 shaped bacteria, an essential component of the elongation machinery is the actin
57 homolog MreB, which forms filaments that bind to the inner surface of the
58 cytoplasmic membrane and interact with the cell-wall synthesis machinery to
59 control cell shape through the insertion pattern of peptidoglycan precursors[9].

60

61 The cytoplasmic membrane is often ignored in discussions of bacterial

62 mechanics. Nonetheless, previous studies hinted at an underappreciated load-
63 bearing capacity of the cytoplasmic membrane in resisting expansion due to
64 turgor pressure. The gain-of-function mutation *mlaA** in *E. coli* results in rapid
65 transfer of phospholipids from the cytoplasmic membrane to the outer
66 membrane during starvation, and this transfer causes the cytoplasmic membrane
67 to shrink by ~20% and detach from the cell wall[10,11]. Once the cytoplasmic
68 membrane of starved *mlaA** cells ruptures, its contents expand in volume to
69 reach approximately the original cell length pre-plasmolysis[10,11]. The ability of
70 these cells to persist in a shrunken state for several minutes, together with the
71 subsequent expansion, suggests that the cytoplasmic membrane alone can bear
72 turgor pressure upon material loss and hence has substantial load-bearing
73 capacity.
74
75 Recent studies have revealed that many other components of the envelope
76 beyond the cell wall can impact cellular mechanical integrity[12]. The outer
77 membrane has stiffness properties similar to those of the cell wall and is critical
78 for maintaining cell viability during rapid changes in external osmolarity[13].
79 Mechanical linkages between the cell wall and outer membrane such as Braun's
80 lipoprotein (Lpp) and OmpA strengthen the cell envelope and determine
81 periplasmic width[14-17]. Mechanosensitive channels in the cytoplasmic membrane

82 enable rapid osmolyte efflux to protect cells against hypoosmotic shocks[17,18].
83 Beyond the envelope itself, deletion of a number of other proteins can impact the
84 stiffness of *E. coli* cells[19]. In particular, disruption of MreB filaments by the
85 antibiotic A22 decreased the resistance of *E. coli* cells to bending[20]. One
86 interpretation of this finding is that MreB forms an ultrastructure that directly
87 increases the mechanical stiffness of the envelope, mimicking the function of its
88 eukaryotic counterpart actin[21]. However, the mechanism by which MreB confers
89 increased bending rigidity could involve its interaction partners within the cell-
90 wall synthesis machinery including MreC, MreD[22], RodA, and RodZ[23,24]. During
91 wall synthesis, MreB filaments translate approximately along the circumferential
92 direction[25-28]. Given this motion, it is currently unclear how mechanical forces
93 could be transmitted from MreB, bound to the inner surface of the cytoplasmic
94 membrane, to the rest of the cell envelope.
95
96 In this study, we investigate the mechanical contribution of MreB to the cell
97 envelope by quantifying cell wall deformation during hyperosmotic shocks.
98 Under moderate shocks that are sufficient to cause plasmolysis,
99 depolymerization of MreB by A22 did not significantly increase cell wall
100 deformation, suggesting that MreB does not directly contribute to envelope
101 stiffness. However, under large-magnitude oscillatory hyperosmotic shocks,

102 cytoplasmic contraction gradually decreased in cells with intact MreB, whereas
103 A22-treated cells with depolymerized MreB maintained the same degree of
104 plasmolysis in each successive shock, indicating that MreB filaments are required
105 to prevent cytoplasmic contraction from the cell wall. Fluorescence microscopy
106 revealed that MreB relocalizes to the cell poles during hyperosmotic conditions,
107 where it drives the formation of structural linkages between the cytoplasmic
108 membrane and the cell wall that enable polar wall synthesis. Perturbations of
109 certain cell-wall synthesis factors altered the coupling, indicating that the
110 elongation machinery forms a physical linkage between the cytoplasmic
111 membrane and the peptidoglycan. Using a mutant with a weak outer membrane,
112 we show that wall-less spheroplasts can transiently remain viable even after the
113 outer membrane ruptures, indicating that the cytoplasmic membrane can bear
114 substantial mechanical stress. Based on these results, we propose that rather than
115 directly strengthening the cell wall, MreB-directed cell-wall synthesis
116 mechanically couples the cytoplasmic membrane and the cell wall, enabling the
117 intrinsic stiffness of the cytoplasmic membrane to contribute to the overall
118 strength of the envelope.

119 **Results**

120

121 **Disruption of MreB polymerization does not alter cell-wall stiffness**

122 The previous observation that A22 treatment decreases the bending rigidity of *E.*
123 *coli* cells[20] on a short time scale before transcriptional reprogramming could occur
124 suggested that MreB might directly impact envelope stiffness. To test this
125 hypothesis, we queried whether MreB polymerization and membrane binding
126 affects other morphological responses to perturbations beyond cell bending.
127 First, we reasoned that if MreB filaments were stress bearing, then their
128 depolymerization would alter the force balance across the cell envelope and
129 hence cell size would change. We quantified the dimensions of cells during
130 steady-state growth in a microfluidic flow cell (Methods) with high temporal
131 resolution before and after addition of 100 μg/mL A22, which rapidly disrupted
132 MreB polymerization as expected (Movie S1). Cell width and length were
133 unaffected (Fig. 1a), indicating that MreB was not bearing levels of longitudinal
134 or circumferential stress relevant to cell morphology.

135

136 Nonetheless, it remained possible that MreB contributes to envelope stiffness by
137 bearing stress when cells experience mechanical perturbations that disrupt
138 steady-state growth. To investigate this possibility, we applied oscillatory

139 osmotic shocks in a microfluidic flow cell and measured the deformation of the
140 cell wall upon each hyperosmotic shock in the absence and presence of A22
141 (Methods). In this assay, log-phase cells were alternately subjected to
142 hyperosmotic (LB+400 mM sorbitol) and normal (LB) osmotic conditions (Fig.
143 1b). Each hyperosmotic shock led to contraction of the cell wall and was
144 sufficiently large in magnitude to reduce turgor pressure to zero, as evidenced by
145 plasmolysis of the cytoplasm (Fig. 1c). The stiffness of the cell envelope is related
146 to the degree of deformation upon removal of turgor[12]. As observed in previous
147 studies with 100-mM shocks[7], the magnitude of length and width contractions
148 was consistent across shock cycles (Fig. 1d). We found that the degree of
149 contraction was not significantly different between cells without or with 10 min
150 of treatment with 100 μg/mL A22 prior to the start of the shocks (Fig. 1d). Thus,
151 disruption of MreB polymerization does not affect the mechanical response of
152 the cell envelope to forces that induce contraction/extension.
153
154 Taken together, these results indicate that MreB does not contribute directly to
155 cell envelope stiffness, despite the significant impact of A22 on bending rigidity[20].
156
157 **MreB promotes a physical coupling between the cytoplasmic membrane to the**
158 **cell wall**

159 Since MreB and its associated components of the cell-wall synthesis machinery
160 form a transmembrane structure connecting the cytoplasmic membrane to the
161 cell wall[29], we reasoned that MreB may prevent detachment of the cytoplasmic
162 membrane from the cell wall during osmotic shocks. To accentuate the impact of
163 A22 treatment, we increased the magnitude of the osmotic shock oscillations to 1
164 M (Methods), which substantially inhibited *E. coli* cell growth (Fig. S1). To
165 counteract the induction of cell division by hyperosmotic shocks[30], we also
166 treated cells with the antibiotic cephalexin (50 μg/mL), which targets the key
167 division protein PBP3[31], in the microfluidic flow cell for 40 min prior to the
168 shocks (Methods). In cells pre-treated with A22 for 10 min, the degree of
169 cytoplasmic contraction was consistently large over the course of 10 osmotic
170 shock cycles (Methods, Fig. 1e). In contrast, in untreated cells, the degree of
171 cytoplasmic contraction gradually decreased over the cycles (Fig. 1e). During the
172 last few shocks, many untreated cells exhibited little plasmolysis (Fig. 1f),
173 suggesting that polymerized MreB gradually inhibited detachment of the
174 cytoplasm from the cell wall. In addition to inhibiting detachment of the
175 cytoplasm from the cell wall, the linkages mediated by MreB also caused the cell
176 wall to buckle under the negative pressure generated by cytoplasmic contraction
177 for 1 M shocks, resulting in thinning of the cylindrical region around midcell
178 (Fig. S2). Treatment with 80 μg/mL MP265, a structural analog of A22, led to

179 similar effects as A22 (Fig. S3, Methods), arguing against potential off-target
180 effects of A22. These findings indicate that MreB promotes physical coupling of
181 the cytoplasmic membrane to the rest of the cell envelope.
182

183 **Plasmolysis results in relocalization of MreB to the cell poles**

184 To probe the dependence of plasmolysis dynamics on oscillatory osmotic shock
185 magnitude, we tracked the subcellular localization of MreB in a strain expressing
186 an MreB-msfGFP sandwich fusion that complements *mreB* deletion[32,33] (Table S1).
187 During steady-state growth, MreB filaments localized primarily to the cylindrical
188 region of the cell (Fig. 2a)[33], as expected, where they guide the insertion of new
189 cell wall material[27]. During 1 M oscillatory osmotic shocks, the first few
190 hyperosmotic shocks induced cytoplasmic contraction mostly near the cell poles
191 (Fig. 2a), indicating the lack of coupling between the cytoplasmic membrane and
192 the rest of the envelope at the poles, where MreB was largely absent. However, in
193 subsequent osmotic shock cycles, MreB partially relocalized to the cell poles,
194 resulting in a more homogeneous distribution of MreB across the cell surface
195 (Fig. 2a-c). This gradual relocalization coincided with the decrease in cytoplasmic
196 contraction (Fig. 1e). In contrast, lower-magnitude (400 mM) osmotic shocks for
197 which cytoplasmic contraction remained constant over shock cycles (Fig. 1e)
198 resulted in less relocalization of MreB (Fig. 2c). Thus, we reasoned that repeated,

199 large-magnitude osmotic shocks led to the formation of MreB-mediated linkages
200 between the cytoplasmic membrane and the other envelope layers at the cell
201 poles that are stable over the 4-min period of the shock cycles, which limited
202 contraction during subsequent shock cycles.
203
204 To test whether hyperosmotic shocks themselves trigger MreB relocalization, we
205 varied the duration of hyperosmolarity and observed nearly identical
206 relocalization trajectories over assay time regardless of the number of shock
207 cycles (Fig. S4). These results indicate that MreB filaments relocalize
208 continuously during plasmolysis and recovery, reflecting a process that depends
209 on the time under osmotic perturbation rather than an acute effect of the shock.
210
211 Taken together, these findings suggest that hyperosmolarity drives relocalization
212 of MreB to the poles, where they appear to establish new physical linkages
213 between the cytoplasmic membrane and cell wall that limit cytoplasmic
214 contraction during subsequent osmotic shocks (Fig. 2d).
215
216 **Peptidoglycan elongation couples the cytoplasmic membrane and cell wall**
217 Since MreB resides solely on the inner surface of the cytoplasmic membrane, we
218 surmised that any physical connection to the cell wall must rely on other cellular

219 components. While many proteins interact with both the cytoplasmic membrane
220 and cell wall, presumably only a subset are critical for maintaining the overall
221 physical coupling between layers. We hypothesized that the most likely
222 candidates would be components of the cell-wall synthesis machinery.
223 Supporting this hypothesis, when we performed oscillatory osmotic shocks with
224 1 M sorbitol in a nutrient-free buffer osmotically balanced with LB (0.85X PBS,
225 Methods), regardless of A22 treatment, cells exhibited plasmolysis without a
226 reduction in cytoplasmic contraction over time (Fig. 3a). These data suggest that
227 linkage between the membrane and cell wall requires cell growth. Repeated
228 osmotic shocks in the nutrient-free media still resulted in MreB relocalization to
229 the poles (Fig. S5), indicating that MreB relocalization is not dependent on wall
230 synthesis and is not sufficient for linking the cytoplasmic membrane to the cell
231 wall.
232
233 To test whether MreB relocalization to the poles leads to polar wall synthesis,
234 rather than the side-wall synthesis typical of normal growth, we performed
235 pulse-chase experiments in cells labeled with 3-[[(7-Hydroxy-2-oxo-2H-1-
236 benzopyran-3-yl)carbonyl]amino]-D-alanine hydrocholoride (HADA), which is
237 inserted into the peptidoglycan at locations of growth[33,34]. During subsequent
238 growth in HADA-free medium (Methods), the ratio of fluorescence at the poles

239 relative to the cell body decayed more rapidly in cells undergoing hyperosmotic
240 shocks, indicating increased polar wall synthesis (Fig. 3b). Thus, polar
241 localization of MreB leads to relocalization of elongation machinery function.
242
243 We next hypothesized that proteins involved in cell-wall synthesis[29] contribute to
244 the membrane-cell wall connection. To identify such factors, we performed
245 oscillatory shocks in combination with genetic or chemical perturbation of
246 elongation-associated targets. First, we overexpressed RodA from an inducible
247 plasmid (Table S1) prior to osmotic shocks (Methods). Opposite to
248 depolymerization of MreB by A22, cytoplasmic contraction was reduced during
249 repeated plasmolysis compared with no induction (Fig. 3c). Overexpression of a
250 dominant-negative mutant $rodA^{D262N}$ (Table S1), which blocks the
251 glycosyltransferase activity of RodA[35], led to a similar phenotype (Fig. S6). These
252 results suggest that increasing the copy number of RodA is sufficient to enhance
253 the coupling between MreB and the cell envelope, regardless of RodA activity.
254
255 To assess the contribution of other elongation-associated PBPs, we inhibited their
256 activity using β-lactam antibiotics, which specifically target transpeptidase
257 function. Inhibition of PBP1A/B by cefsulodin, PBP2 by mecillinam, or all PBPs
258 by ampicillin had no effect on cytoplasmic contraction during the shocks (Fig.

259 S7), suggesting that transpeptidase function is not required for establishing the
260 cytoplasmic membrane–cell wall connection.
261
262 To probe the role of glycan strand synthesis, we focused on a deletion mutant of
263 *mltG* (Table S1), which encodes a cytoplasmic membrane-anchored enzyme
264 implicated in the termination of peptidoglycan synthesis[36]. Deletion of *mltG* is
265 predicted to enhance the association of the elongation machinery with the cell
266 wall and results in longer glycan strands[36]. Under oscillatory osmotic shocks,
267 Δ*mltG* cells exhibited a slower transition to the state of lower cytoplasmic
268 contraction compared with wild-type cells (Fig. 3f). Given the role of MltG in
269 termination[37], we reasoned that the accumulation of synthases at the cell poles
270 necessary for reducing cytoplasmic contraction was delayed in Δ*mltG* cells.
271
272 Taken together, these findings highlight the functional duality of the elongation
273 machinery in both cell-wall synthesis and as a mechanically robust connection
274 between the cytoplasmic membrane and the cell wall.
275
276 **The cytoplasmic membrane has substantial load-bearing capacity**
277 Our findings collectively suggest that MreB does not directly contribute to
278 envelope stiffness, and instead promotes physical coupling between the

279 cytoplasmic membrane to the cell wall via its role in cell-wall synthesis. This
280 linkage is unlikely to provide substantial stiffness in the longitudinal or
281 circumferential directions along the surface of the cell, since the direction of
282 forces exerted to link the layers would be predominantly perpendicular to the
283 surface. However, if the cytoplasmic membrane itself were load bearing, such a
284 coupling could explain the substantial decrease in bending rigidity under A22
285 treatment[20], wherein MreB (and the coupling it promotes) is required for bending
286 to engage the mechanical response of the cytoplasmic membrane (Fig. 4a). While
287 it is typically assumed that the cytoplasmic membrane is relatively flexible
288 compared to the cell wall by virtue of it being a lipid bilayer[12,38], previous
289 molecular dynamics simulations suggested that a protein-rich membrane patch
290 mimicking the cytoplasmic membrane can exhibit substantial stiffness
291 comparable to that of the cell wall and the outer membrane[39].
292
293 To directly test the capacity of the inner membrane to bear stress, we sought to
294 reduce or remove the stress-bearing capacity of the cell wall and outer
295 membrane. Cell wall-free spheroplasts can be generated with lysozyme[40].
296 However, the outer membrane is thought to be essential, potentially due to
297 osmotic balancing in the periplasm[17], and no mechanism currently exists for
298 robustly removing the outer membrane while retaining cell viability[12]. Thus, we

299 leveraged our previous finding that deletion of *bamD* results in a highly
300 mechanically compromised outer membrane due to a drastic reduction in outer
301 membrane protein levels[41]. We successfully generated wall-free Δ*bamD*
302 spheroplasts using 20 μg/mL lysozyme, indicating that even without a cell wall,
303 at least some cells with a highly mechanically compromised OM can persist in a
304 rich medium without osmoprotection (Fig. 4b).
305
306 To monitor changes to the cell envelope during and after cell-wall digestion, we
307 tracked Δ*bamD* cells expressing cytoplasmic GFP and periplasmic mCherry in a
308 microfluidic flow cell (Methods). Upon lysozyme introduction, cells lost their rod
309 shape and became spherical (Fig. 4c). Without the stiff cell wall that typically
310 bears turgor pressure, the mechanical load shifted to the two membranes,
311 resulting in a ~20% increase in the surface area of the cytoplasmic membrane
312 (Fig. 4d, Methods). Approximately half of Δ*bamD* spheroplasts persisted for >10
313 min with an expanded cytoplasmic membrane before lysis, highlighting the
314 ability of the membrane to bear turgor pressure. The spheroplasts survived for a
315 shorter period compared to in a liquid environment (Fig. 4b), likely due to the
316 mechanical confinement of the thin microfluidic flow cell. During the process of
317 lysis, Δ*bamD* spheroplasts lost the periplasmic mCherry signal earlier than or
318 simultaneously with the loss of cytoplasmic GFP (Fig. 4c), indicating that the

319 outer membrane ruptured before or at the same time as the cytoplasmic
320 membrane. After outer membrane rupture, ~50% of spheroplasts persisted with
321 an intact cytoplasmic membrane for >5 min. In these cells, outer membrane
322 rupture caused almost no change in the cytoplasm area (Fig. 4e), suggesting that
323 the turgor pressure was borne solely by the cytoplasmic membrane rather than
324 the mechanically compromised outer membrane. These findings provide direct
325 evidence of the load-bearing capability of the cytoplasmic membrane, such that
326 when coupled to the cell wall by the process of cell-wall synthesis, the
327 cytoplasmic membrane can increase the stiffness of the cell envelope.

328 **Discussion**

329 In this study, we provide a revised perspective on the origins of mechanical
330 resilience of the cell envelope, and demonstrate that the cell-wall synthesis
331 machinery has a dual catalytic–structural function in integrating growth with
332 envelope mechanics. We found that MreB does not contribute directly to cell wall
333 stiffness under repeated plasmolysis (Fig. 1a,d) but instead functions as a
334 platform for the components of the cell-wall synthesis machinery to link the
335 cytoplasmic membrane and the cell wall sufficiently strongly as to prevent
336 plasmolysis. Fluorescently labeled MreB filaments relocalized to the cell poles
337 during large-magnitude osmotic shocks (Fig. 2), which in turn limited
338 cytoplasmic contraction in these regions during periods of hyperosmolarity and
339 led to peptidoglycan synthesis at the poles (Fig. 3b) as long as nutrients were
340 available (Fig. 3a). Among the many components involved in cell-wall
341 elongation, overexpression of RodA (Fig. 3c) and removal of MltG (Fig. 3e)
342 impacted the connection between the cytoplasmic membrane and cell wall.
343 Motivated by these findings and our evidence of substantial load-bearing
344 capacity of the cytoplasmic membrane (Fig. 4), we propose a biophysical model
345 in which MreB and active peptidoglycan synthesis are necessary for
346 mechanically coupling the cytoplasmic membrane to the rest of the cell envelope.
347 This model provides an explanation for the previously observed changes in

348 bending rigidity during A22 treatment[20]: with intact MreB filaments, the
349 cytoplasmic membrane can contribute to resisting bending. In fact, the ~30%
350 decrease in bending rigidity during A22 treatment is in line with expectations
351 based on detaching a single layer from an envelope with three layers of roughly
352 equal mechanical importance.
353
354 The proteins that physically link bacterial surface layers are often critical to
355 cellular mechanical integrity. Braun's lipoprotein (Lpp) and certain β-barrels
356 connect the OM to the cell wall and impact the ability of the outer membrane to
357 bear load under compression[13]. Lpp also regulates periplasmic width and the
358 stiffness of *E. coli* cells[14]. However, the linkages between the cell wall and the
359 cytoplasmic membrane have largely been overlooked, in part due to the lack of
360 suitable assays for interrogating this connection. Our findings highlight the
361 dynamic nature of the cytoplasmic membrane-peptidoglycan linkage. High-
362 magnitude oscillatory osmotic shocks induced linkage formation at otherwise
363 uncoupled cell poles, a process dependent on the relocalization of MreB and
364 repositioning of at least certain components of the elongation machinery. The
365 linkages, which are likely transient rather than persisting as static structures,
366 may rely on several factors. While an obvious candidate is crosslinked glycans,
367 our results suggest that, although they may contribute, they are not required.

368 RodA does not extend far enough into the periplasm to bind peptidoglycan,
369 suggesting that other factors such as RodZ or MreC mediate the connection.
370 Potential redundancy or decoupling of the activity and binding of the factors
371 involved may complicate elucidating the precise makeup and dynamics of the
372 coupling. Nonetheless, it is striking that A22 treatment alone is sufficient to alter
373 cytoplasmic contraction under repeated osmotic shocks (Fig. 1E), highlighting
374 the key role of MreB in organizing the peptidoglycan synthesis machinery.
375
376 One open question raised by our work is the mechanism by which MreB
377 relocalizes to the cell poles during large hyperosmotic shocks. Previous studies
378 found that MreB is enriched in log-phase cells at regions of the membrane with
379 negative mean curvature[33,42], which has been hypothesized to underlie a feedback
380 control mechanism for maintaining rod-like shape[9]. Plasmolysis generates
381 regions of negative mean curvature near the poles, as indicated by the
382 cytoplasmic membrane dye MitoTracker Green[43,44] (Fig. S8a), and cytoplasmic
383 contraction could generate wrinkles in the membrane with large absolute
384 curvature that could either bias the localization of MreB filaments based on
385 geometric preference or by disrupting their circumferential motion[45]. However,
386 MreB relocalized to cell poles at a rate independent of whether obvious
387 plasmolysis occurred at that pole (Fig. S8b), indicating that at least large

388 deformations are not necessary for relocalization. Regardless of the mechanism,
389 the ability of MreB to target distinct regions of the cell depending on
390 environmental cues such as osmolarity may provide bacterial cells with
391 morphological flexibility. This flexibility is apparent during the transition into
392 and out of stationary phase, during which MreB also exhibits polar localization[24],
393 which our study suggests could be due to osmolarity changes.
394
395 In addition to mechanically strengthening the cell envelope, linkages between
396 surface layers control the distance between layers[14], which can be critical for the
397 function of proteins that span the space[46-48]. In the case of MreB, the cell-wall
398 synthesis-mediated linkages are mostly present only along the cylindrical cell
399 body during log-phase growth. Thus, during a small osmotic perturbation, the
400 cell poles can function as a temporary buffer for water efflux, while the distance
401 between the cytoplasmic membrane and the cell wall along the rest of the
402 cylindrical body is not affected, allowing for continued growth even in the
403 absence of turgor[13,49]. In the future, it will be interesting to determine whether
404 MreB-directed cell-wall synthesis plays a similar mechanical function in other
405 species. Regardless, a deeper understanding of the mechanical interactions
406 between the cytoplasmic membrane and the cell wall provides new insights into

407 the structural stability of the cell envelope and reveals potential targets and

408 mechanisms for antimicrobial intervention.

409 **Methods**

410

411 **Bacterial strains and growth conditions**

412 All strains and plasmids used in this study are listed in Table S1. *E. coli* cells were
413 grown overnight in lysogeny broth (LB, Lennox, Fisher Scientific, Cat. #BP9722-
414 500) at 37 °C, diluted into fresh LB, and grown for 2 h into log phase for
415 microfluidic measurements. Strains were grown with 50 μg/mL kanamycin
416 (Sigma-Aldrich, Cat. #K4000) or 50 μg/mL chloramphenicol (Calbiochem, Cat.
417 #220551) as necessary.

418

419 The Δ*mltG* strain expressing cytoplasmic GFP was generated by λ-Red
420 recombination using pSIM6. A chloramphenicol resistance cassette (cmR)
421 flanked by FRT sites was PCR-amplified from pKD3 with primers containing the
422 same 50-nt homology overhangs upstream and downstream of *mltG* as the Keio
423 collection[50] (forward primer: 5′-
424 ACGTTATATGAATATTTAGCCCCACTTTGTGAGCGCCCGAATTAGTCATGt
425 ccatatgaatatcctccttagttcctattcc-3′; reverse primer: 5′-
426 CGCCTTCCAGCCCCTCAATGACGATATACTTACTGCGCATTTTTTTCCTTtgt
427 aggctggagctgcttcg-3′). The PCR product was electroporated into BW25113
428 carrying pSIM6, and recombinants were selected on LB agar with 50 μg/mL

429 chloramphenicol. The strain was subsequently transformed with pZS21-GFP
430 (Table S1) to drive constitutive GFP expression.
431
432 **Microfluidic hyperosmotic shock assays**
433 Cells from a saturated culture grown overnight were diluted 1:200 into fresh LB
434 and grown at 37 °C for 2 h. These log-phase cells were cultured with 25 μg/mL
435 wheat germ agglutinin (WGA) conjugated to AlexaFluor-555 (AF555, Invitrogen
436 W32464) to label the outer membrane. Cells were then loaded into CellASIC
437 ONIX microfluidic flow cells (Sigma-Aldrich, Cat. #B04A-03-5PK), in which
438 media were exchanged using the CellASIC ONIX2 microfluidic platform (Sigma-
439 Aldrich, Cat. #CAX2-S0000). Oscillatory hyperosmotic shock assays were
440 performed at room temperature.
441
442 Cells were first perfused with LB for 30 min with 50 μg/mL cephalexin (MP
443 Biomedicals, Cat. #150585) to inhibit cell division and then treated with 100
444 μg/mL A22 (gift from Douglas Weibel), 80 μg/mL MP265 (MedChemExpress,
445 Cat. #HY-131583), a beta-lactam antibiotic (100 μg/mL ampicillin (RPI, Cat.
446 #A40040), 50 μg/mL mecillinam (Sigma-Aldrich, Cat. #33447), or 30 μg/mL
447 cefsulodin (MP Biomedicals, Cat. #198677), or 0.85X PBS (Gibco, Cat. #70011044)
448 for 10 min to perturb cell-wall synthesis. Cells were then subjected to oscillatory

449 hyperosmotic shocks involving 400-, 600-, or 1000-mM sorbitol (Sigma-Aldrich,
450 Cat. #S1876, dissolved in LB or 0.85X PBS) and recovery without sorbitol, with a
451 period of 4 min (2 min shock and 2 min recovery). Pre-treatment compounds
452 (A22, MP265, beta-lactam, or 0.85x PBS) were maintained during osmotic shocks.
453 Cells were stained with 25 μg/mL WGA-AF555 throughout incubation in the
454 flow cell.
455
456 To overexpress RodA or $RodA^{D262N}$ (Table S1), cells were induced with 1 mM
457 IPTG (Sigma-Aldrich, Cat. #I6758) for 1 h in liquid culture before loading to the
458 microfluidic flow cell. After loading, cells were incubated with 1 mM IPTG for an
459 additional 30 min, and IPTG was maintained throughout subsequent osmotic
460 shock assays.
461
462 **Fluorescent labeling of peptidoglycan and cytoplasmic membrane**
463 A saturated culture grown overnight in LB medium was diluted 1:200 into LB
464 medium containing 1 mM HADA (MedChemExpress, Cat. #HY-131045/CS-
465 0124027) and grown at 37 °C for 2 h to ensure homogenous peptidoglycan
466 labeling. Cells with fluorescently labeled peptidoglycan were then loaded into
467 microfluidic flow cells and grown in LB with 1 mM HADA at room temperature,
468 followed by hyperosmotic shocks with 1 mM HADA. Cells were then switched

469 to HADA-free LB medium to track peptidoglycan synthesis as indicated by the
470 decay of HADA signals.
471
472 To visualize the cytoplasmic membrane during osmotic shocks, cells were
473 labeled with 2 μg/mL MitoTracker Green (Invitrogen, Cat. #M7514) in liquid
474 culture and in the microfluidic flow cell.
475
476 **Single-cell imaging**
477 Cells undergoing oscillatory hyperosmotic shocks were monitored using a Nikon
478 Eclipse Ti-E inverted epifluorescence microscope with a 100X (NA 1.40) oil-
479 immersion objective (Nikon Instruments). Phase-contrast and fluorescence
480 images were collected on a Prime BSI Express sCMOS camera (Teledyne
481 Photometrics) using *μManager* v. 2.0[51].
482
483 **Image analysis**
484 Time-lapse images were segmented with the machine learning-based software
485 *DeepCell*[52] trained on WGA-stained cells, and the segmented images were
486 analyzed using *Morphometrics*[52] to obtain cell contours at sub-pixel resolution.
487 Using these contours, single-cell lineages were tracked. Cells that were
488 segmented or tracked incorrectly or that lysed during osmotic shocks were

489 filtered out via manual inspection. Cell length and width were calculated using
490 the *MicrobeTracker*[53] meshing algorithm. Cytoplasmic area was inferred using
491 cytoplasmic GFP fluorescence, and cytoplasmic contraction during plasmolysis
492 was computed based on the fraction of the total area enclosed by the cell contour
493 represented by the cytoplasmic area.
494
495 To determine the spatial localization of MreB filaments in cells expressing MreB-
496 GFP, in Fig. 2b, fluorescence profiles along cell contours were calculated as
497 previously described[54] and the degree of fluorescence along the cylindrical region
498 and the cell poles was compared. In Fig. 2c, S4, and S6b, the average fluorescence
499 intensity was calculated for the projected cylindrical region and both cell poles,
500 where the highly curved polar regions were defined based on a curvature
501 threshold.
502
503 **Cell shape analysis**
504 Cell wall area contraction in Fig. 1d was calculated as (area plasmolysis
505 contraction)/(area after plasmolysis)–1. Cytoplasmic area expansion in Fig. 4e
506 was calculated as (area after OM rupture)/(area before OM rupture)–1. Cell
507 width was extracted from the pill mesh generated by the *MicrobeTracker*[53]
508 meshing algorithm and defined as the maximum width measured perpendicular

509 to the cell's long axis. Cell width increase in Fig. S3b was calculated as (width
510 under shock)/(width prior to shock)–1.
511
512 The cytoplasmic membrane area in Fig. 4d was calculated separately for rod-
513 shaped cells prior to wall digestion and for spheroplasts after digestion using the
514 same approximation as in ref. [13]. Cell contours were generated using
515 *Morphometrics*[52] from cytoplasmic GFP fluorescence. For rod-shaped cells, the
516 membrane area was estimated from the contour assuming rotational symmetry
517 around the long axis. For spheroplasts, which adopted amorphous shapes within
518 the thin flow cell, the flow cell height was assumed equal to the cell width prior
519 to wall digestion, w. The projected area, a, and perimeter, s, were calculated from
520 the contour, and the cytoplasmic membrane area was then estimated as $2a+ws$.
521
522 **Spheroplast generation**
523 To generate cell wall-free spheroplasts with a compromised OM, Δ*bamD* cells
524 (Table S1) were grown in LB for 2 h and treated with 100 μg/mL lysozyme
525 (Sigma-Aldrich, Cat. #L6876) in LB. To generate and monitor spheroplasts in a
526 microfluidic flow cell, Δ*bamD* cells were treated with 100 μg/mL lysozyme in LB.
527 Expression of periplasmic mCherry was induced with 1 mM IPTG.
528

Data and code availability

All data used for generating figures in this study are available at the Stanford Digital Repository: https://purl.stanford.edu/gg063dh4581.

Figures

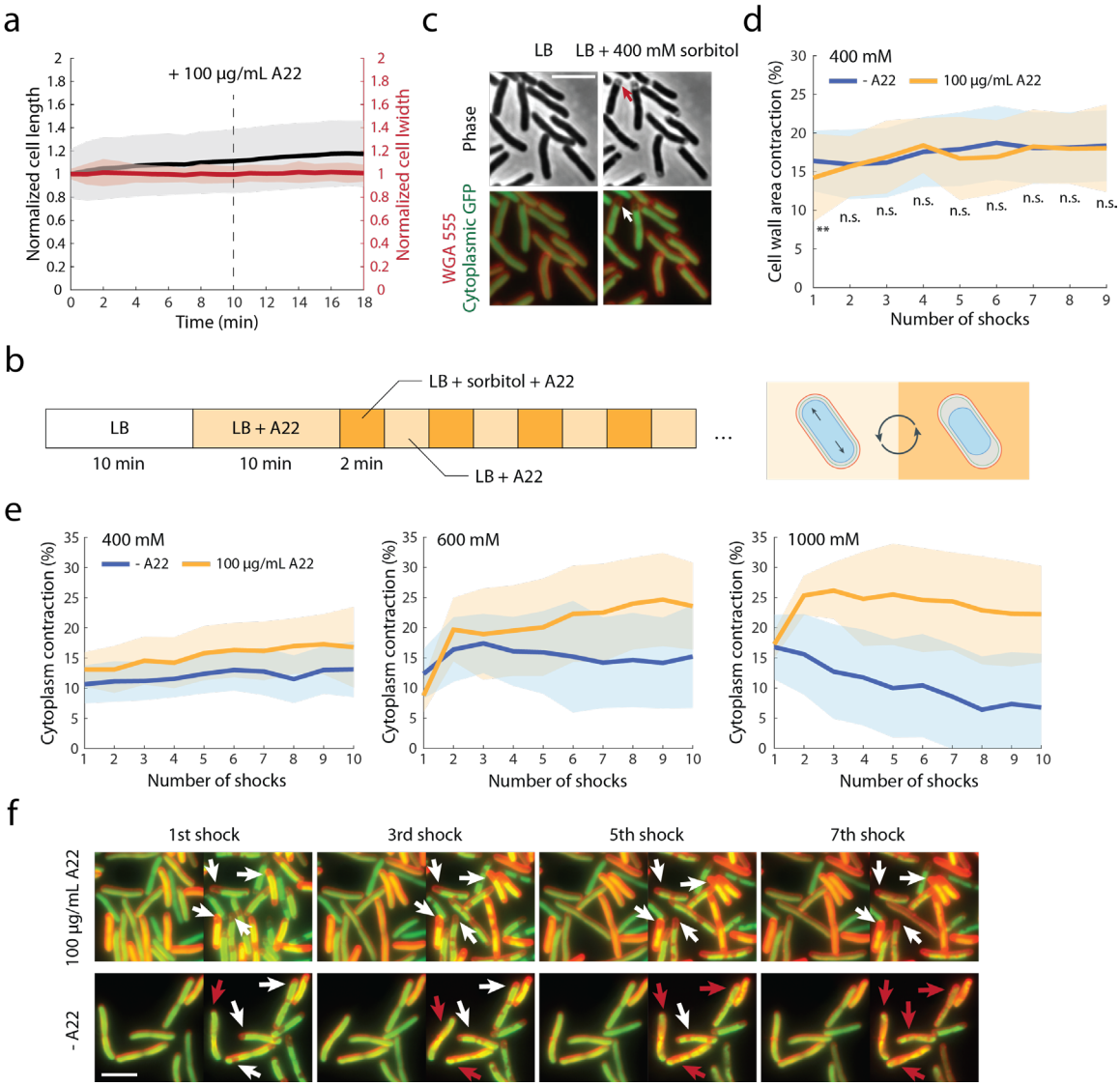

Figure 1: MreB couples the cytoplasmic membrane to the cell wall.

a) Disruption of MreB filaments with 100 µg/mL A22 in LB medium did not alter cell length or width, suggesting that MreB filaments are not under stress during exponential growth. A22 treatment started at $t = 10$ min.

b) Schematic of the oscillatory hyperosmotic shock assay in which cells

540 were periodically subjected to hyper- and normal osmolarity
541 (Methods). Under normal osmolarity, the cell wall is under tension due
542 to turgor pressure; under hyperosmolarity, the cytoplasm loses water
543 and detaches from the cell wall.

544 c) Exposure to 400 mM hyperosmotic shock cycles led to cytoplasmic
545 contraction, typically seen at the cell poles (red/white arrows highlight
546 one example). The OM and the cytoplasm are labeled with wheat germ
547 agglutinin (WGA) AlexFluor-555 and GFP expressed from a plasmid,
548 respectively. Scale bar: 5 μm.

549 d) Disruption of MreB filaments via pre-treatment with 100 μg/mL A22
550 did not alter cell wall contraction (Methods) under 400 mM oscillatory
551 hyperosmotic shocks. **: $p < 0.01$, n.s.: $p > 0.01$; Welch's t-test was
552 performed for each osmotic shock cycle.

553 e) Inhibition of cytoplasmic contraction by MreB in plasmolyzed cells
554 was dependent on the number and magnitude of the oscillatory
555 osmotic shocks. The impact of A22 pre-treatment on cytoplasmic
556 contraction was prominent only under large hyperosmotic shocks (600
557 mM and 1 M).

558 f) The presence of MreB filaments resulted in mechanical coupling
559 between the cytoplasmic membrane and the cell wall (red arrows);

560 disruption of MreB by A22 allowed unhampered plasmolysis (white
561 arrows). Cells are labeled with WGA AF-555 and cytoplasmic GFP
562 expressed from a plasmid. Scale bar: 5 μm.

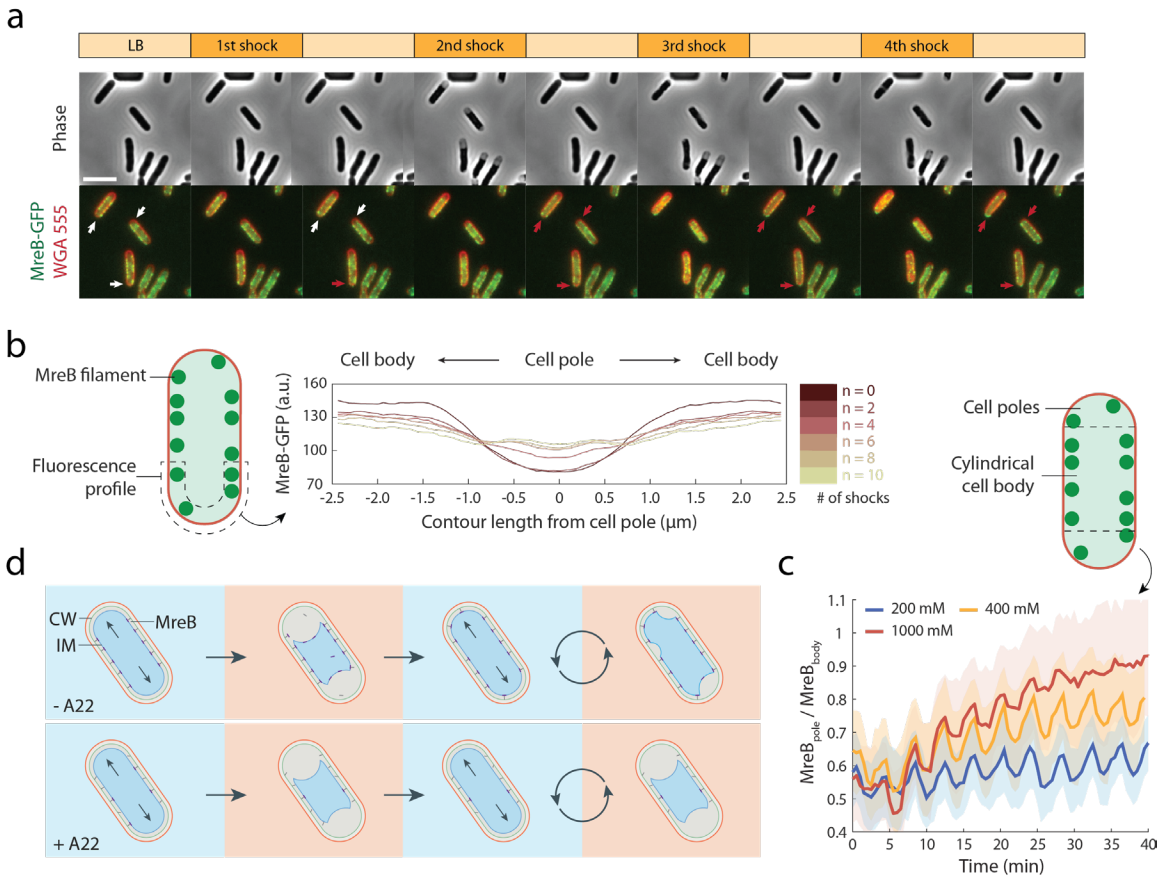

Figure 2: Hyperosmolarity causes relocalization of MreB filaments to the poles.

a) 1-M oscillatory osmotic shocks resulted in relocalization of MreB-msfGFP filaments to cell poles (red arrows), which are generally depleted of MreB-msfGFP during normal growth (white arrows). Scale bar: 5 μm.

b) MreB-msfGFP profiles of individual cell poles, averaged across the contours of *n*=348 cells, demonstrate the increasingly homogenous distribution of MreB after more 1-M hyperosmotic shocks. The profiles span the pole and surrounding region (left schematic).

573 c) The increase in the ratio of MreB-msfGFP intensity at the cell poles
574 compared to the cylindrical cell body (left schematic) demonstrates the
575 relocalization of MreB to the poles. The degree of relocalization was
576 dependent on the shock magnitude. The sawtooth behavior is due to
577 repeated plasmolysis and subsequent recovery.
578 d) Schematic of MreB relocalization under hyperosmotic shocks and
579 formation of new mechanical linkages at the cell poles.

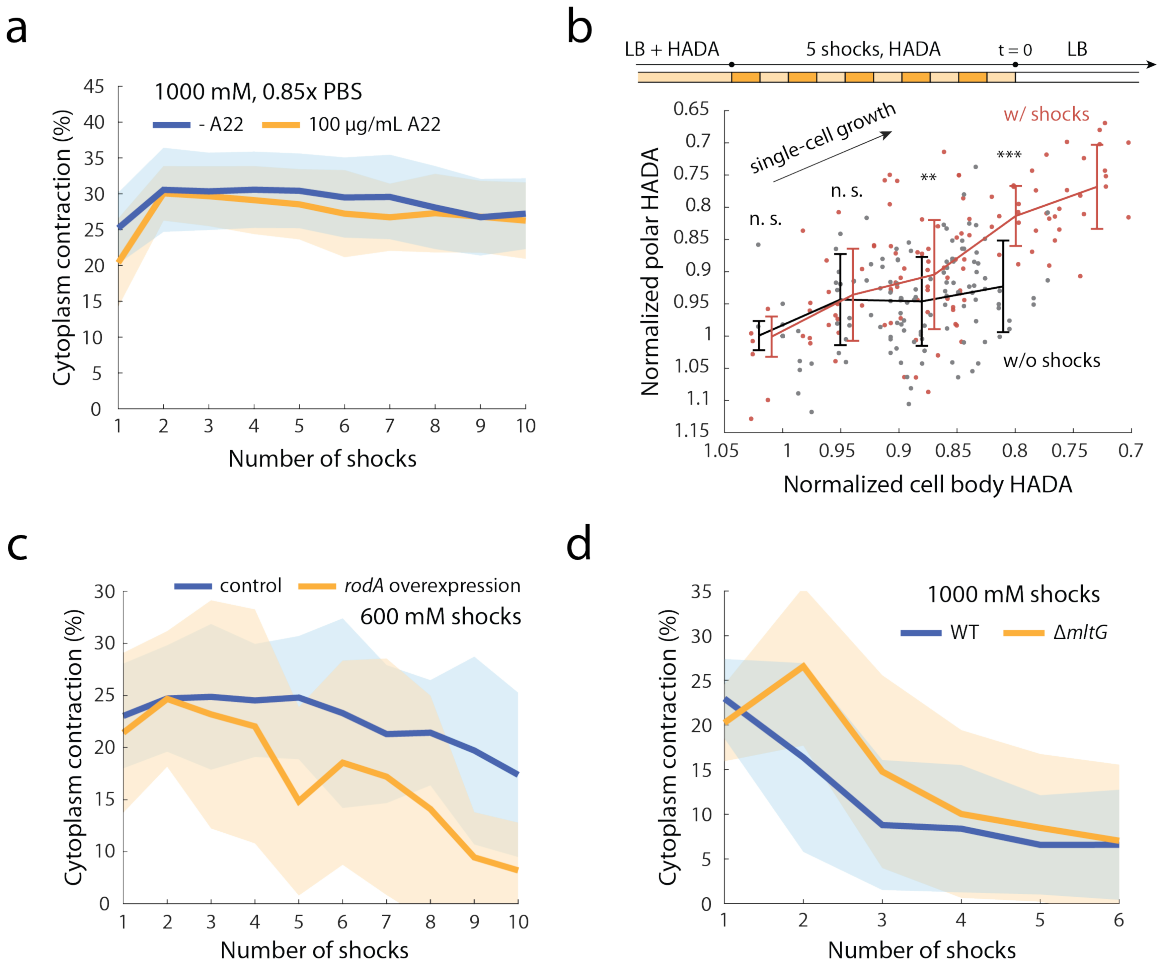

Figure 3: Inactivation of cell-wall synthesis alters the coupling between the cytoplasmic membrane and the peptidoglycan.

a) In 0.85X PBS, wild-type cells exhibited plasmolysis without any reduction in cytoplasmic contraction over repeated 1-M osmotic shocks, regardless of A22 treatment.

b) Pulse-chase experiment in cells pre-labeled with 1 mM HADA. Compared to cells grown without shocks, cells exposed to shocks exhibited greater decreases in fluorescence at the poles, when

589 evaluated at the same level of fluorescence decay in the cell body,
590 indicating increased polar peptidoglycan synthesis following osmotic
591 shock-induced MreB relocalization. Top: schematic of the HADA
592 labeling and hyperosmotic shock protocol. Cells were tracked in a
593 microfluidic flow cell during growth without HADA starting at t=0.
594 Each data point corresponds to an individual cell pole. $N \geq 25$ cells were
595 tracked for each condition. **: $p < 0.01$, ***: $p < 0.001$, n.s.: $p > 0.01$;
596 Welch's t-test was performed on binned data points.
597 c) Overexpression of RodA reduced cytoplasmic contraction during 600-
598 mM osmotic shocks.
599 d) Δ*mltG* cells exhibited a slower transition to the coupled state compared
600 to wild type during 1-M shocks. The degree of contraction was
601 significantly different (Welch's t-test: $p < 0.01$) in the first 3 shocks and
602 similar after n>3 shocks.

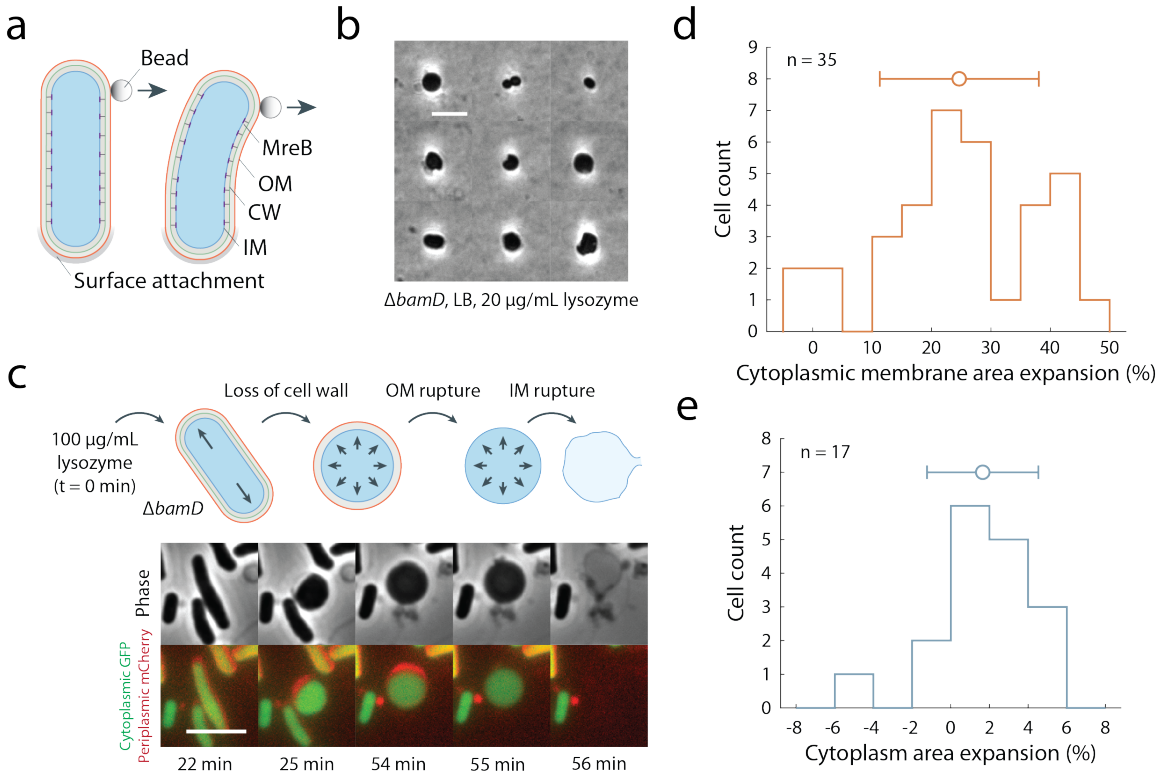

Figure 4: The cytoplasmic membrane has the capacity to bear substantial mechanical stress.

a) MreB-mediated coupling between the cytoplasmic membrane and the cell wall may explain the decrease in bending rigidity of *E. coli* cells upon A22 treatment[20] if the cytoplasmic membrane is sufficiently stiff.

b) Spheroplasts without a cell wall can be generated from Δ*bamD* cells with weak outer membranes using 20 µg/mL lysozyme in LB medium without additional osmoprotection. Cells were imaged 3 h after lysozyme treatment (Methods). The panel shows a composite of representative snapshots of individual spheroplasts. Scale bar: 5 µm.

c) Schematics and images during the generation of Δ*bamD* spheroplasts,

615 rupture of the weakened outer membrane, and lysis due to inner
616 membrane rupture. Δ*bamD* cells were labeled with cytoplasmic GFP
617 and periplasmic mCherry and tracked in a microfluidic flow cell
618 (Methods). Loss of periplasmic mCherry signal indicates rupture of the
619 outer membrane, which always occurred prior to or at the same time
620 as cytoplasmic membrane rupture. Scale bar: 5 μm.

621 d) The surface area of the cytoplasmic membrane increased when the cell
622 wall was degraded, indicating that the remaining envelope layers
623 (cytoplasmic and outer membranes) bore more of the stress due to
624 turgor pressure in the absence of the wall. *n*=35 cells.

625 e) Rupture of the outer membrane in Δ*bamD* spheroplasts resulted in
626 only a slight increase in cytoplasmic area, suggesting that the outer
627 membrane was not bearing substantial stresses in the spheroplasts.
628 *n*=17 cells.

629 **Supplementary Figures**

630

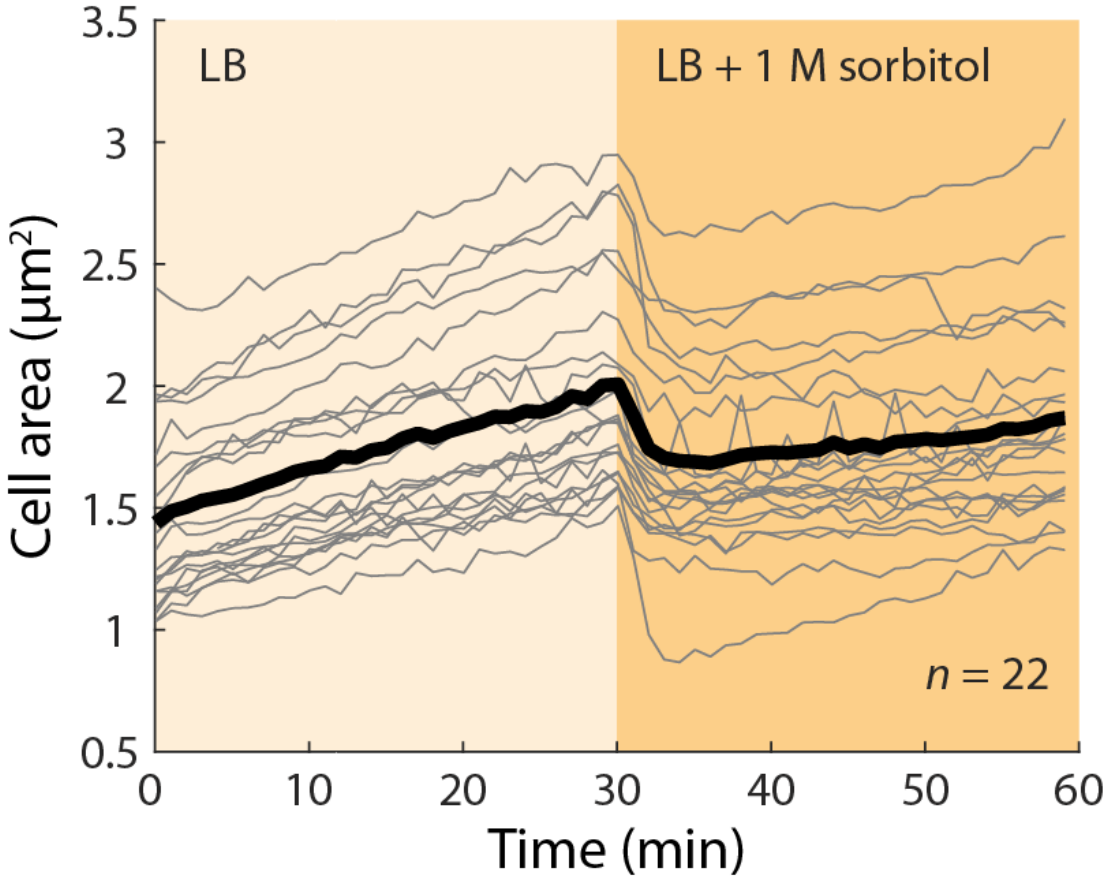

631

632 **Figure S1: Cell growth is inhibited under large hyperosmotic shocks.**

633 During a hyperosmotic shock with 1 M sorbitol in LB, cell growth was inhibited

634 for an extended period. Cells were monitored in a microfluidic flow cell

635 (Methods). *n*=22 cells.

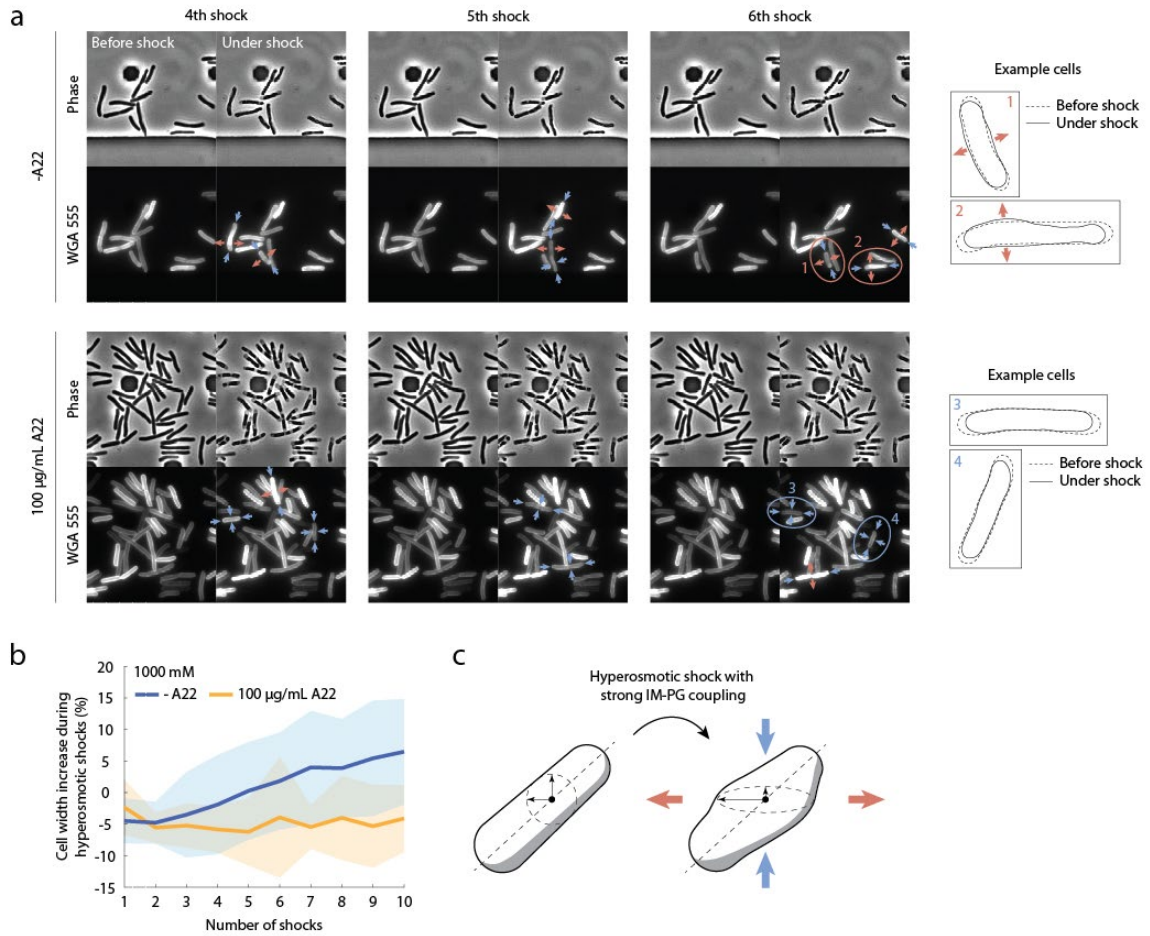

Figure S2: When mechanically coupled to the cytoplasm, the cell wall exhibits large deformations and increases in cell width during large hyperosmotic shocks.

a) After several osmotic shock cycles (1 M sorbitol in LB), when the cell wall is mechanically coupled with the cytoplasmic membrane by MreB filaments, the cell wall becomes flattened by the negative osmotic pressure from inside the cytoplasm under high environmental osmolarity, resulting in increased cell width around midcell. These large deformations only occurred under large (600 mM or 1 M) osmotic shocks.

646 b) Cell width increased after several 1-M hyperosmotic shock cycles. This
647 widening was abolished by A22 pre-treatment, with cells contracting in
648 width upon loss of turgor.
649 c) Schematic of cell flattening caused by the mechanical linkages and
650 osmotic pressure. Red and blow arrows indicate extension and
651 compression along different axes of the cross-section.
652

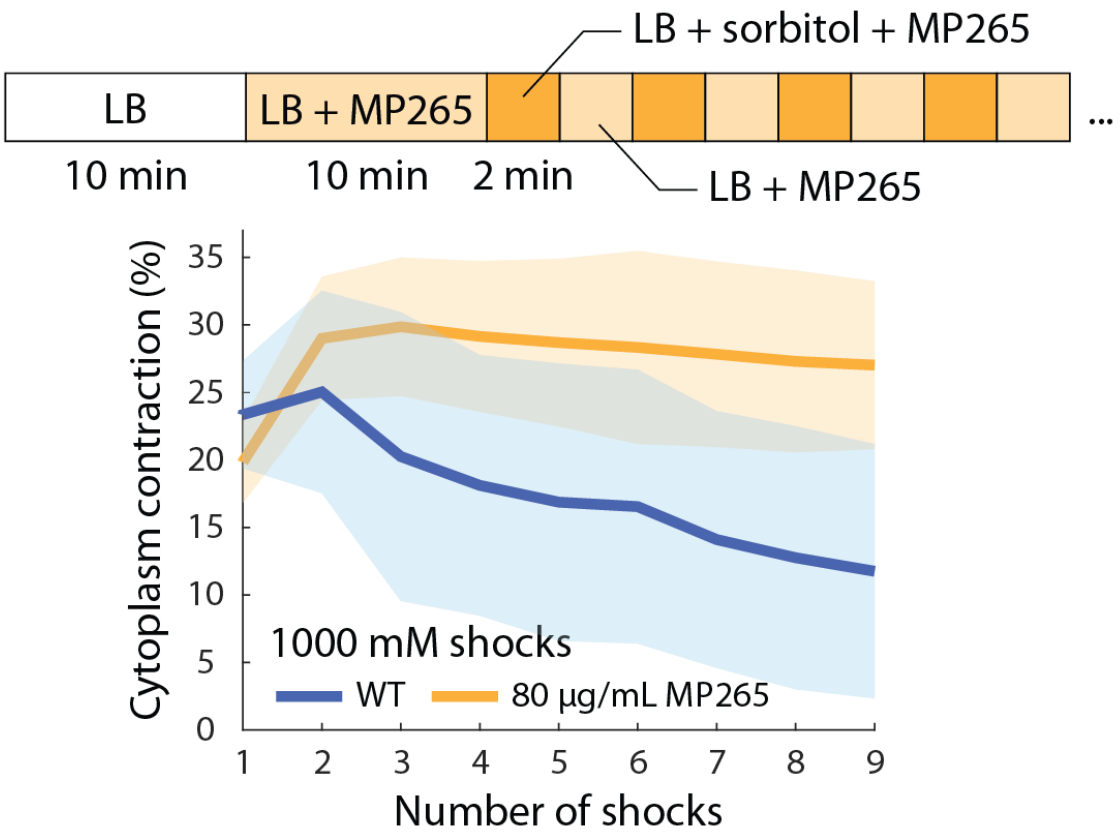

Figure S3: Disruption of MreB filaments with MP265 eliminates the mechanical coupling between the cytoplasmic membrane and the cell wall during oscillatory osmotic shocks. Wild-type cells were treated with 80 µg/mL MP265 10 min prior to and during 1-M osmotic shocks. The lack of coupling is similar to the effects of A22 treatment (Fig. 3e).

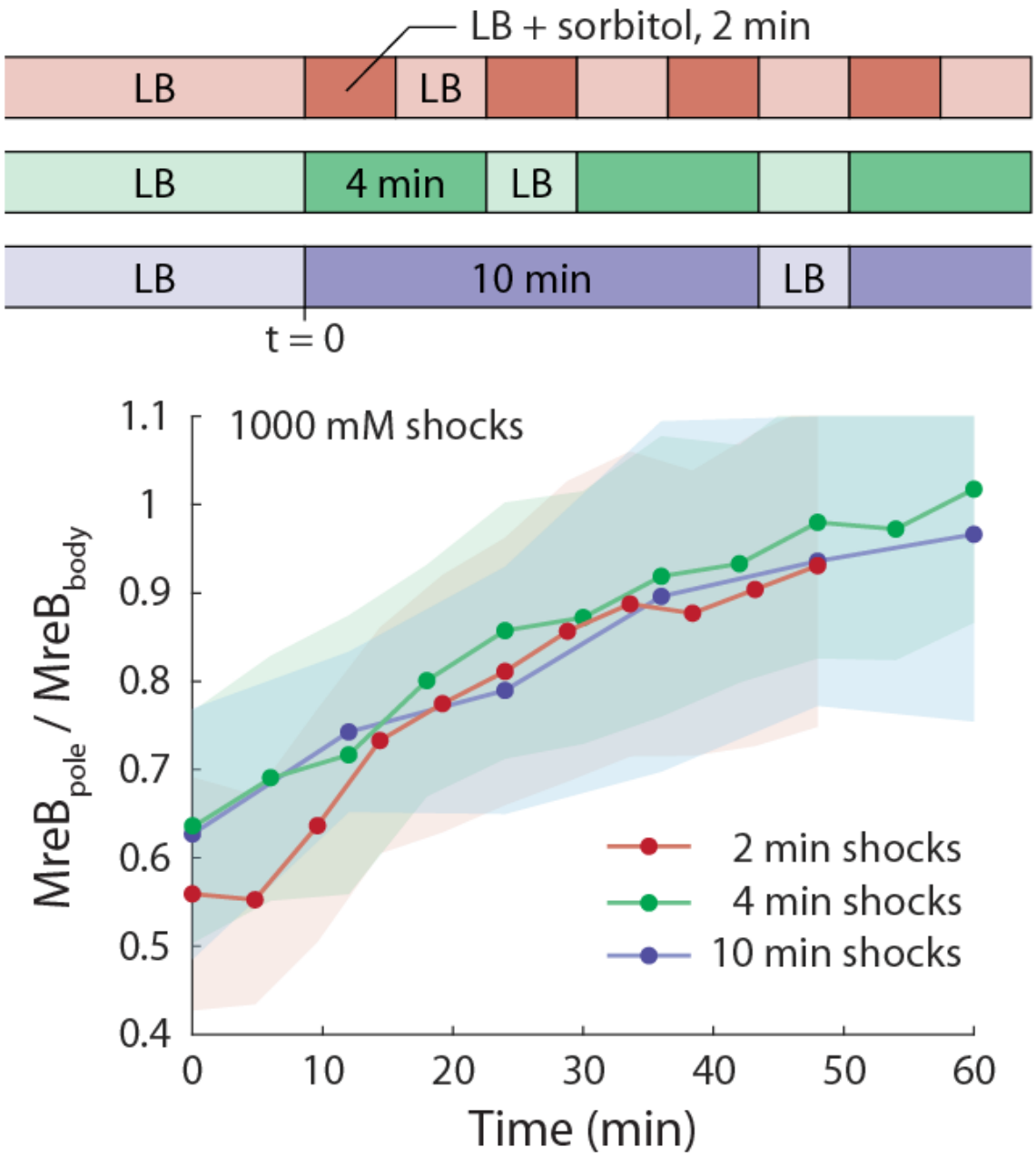

Figure S4: MreB relocalization to the poles is determined by the time under osmolarity oscillation rather than the number of shock cycles. Hyperosmotic shocks with extended periods (4 min, 10 min) of hyperosmolarity (upper schematic) resulted in similar degrees of MreB relocalization as with a 2-min

664 period for a given assay time. Data points represent individual osmotic shock

665 cycles. Fluorescence was evaluated during times of normal osmolarity to avoid

666 bias caused by plasmolysis.

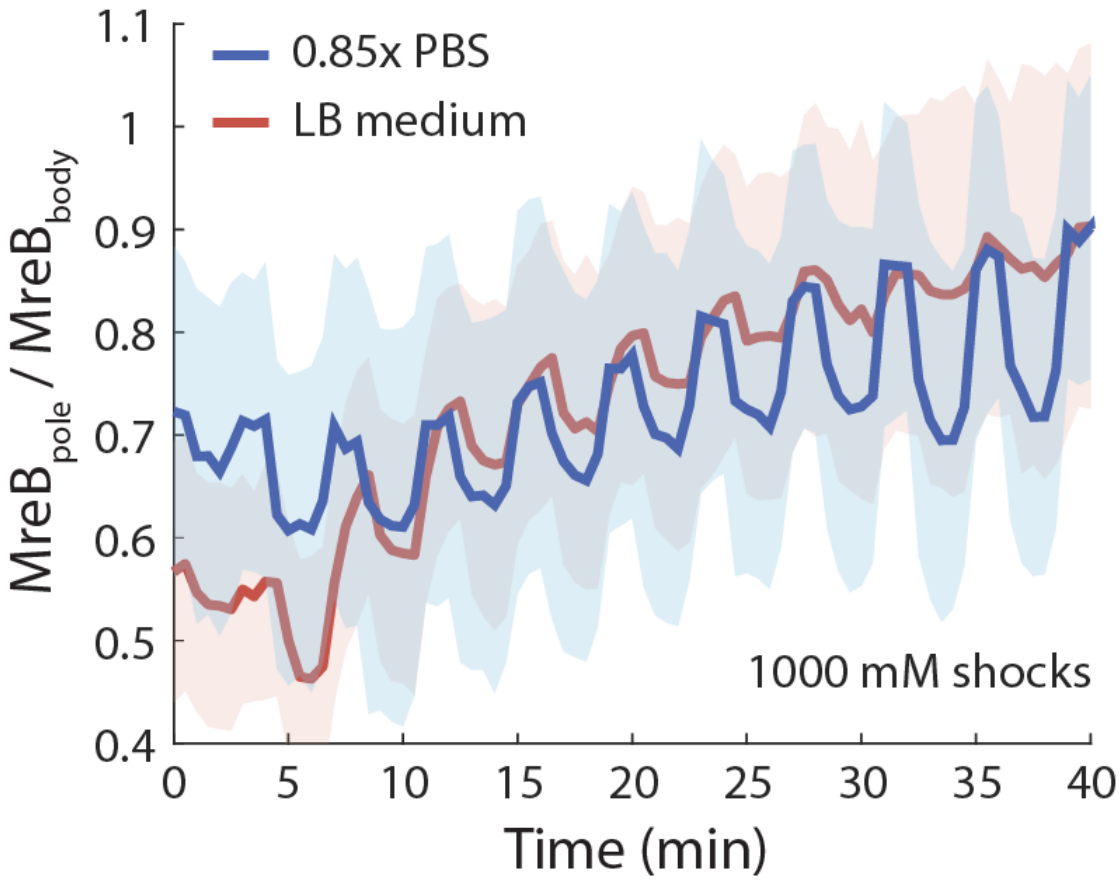

Figure S5: MreB relocalizes to the poles during oscillatory osmotic shocks in a nutrient-free buffer. In 0.85X PBS, MreB relocalization due to osmotic shocks progressed at a similar rate as in LB.

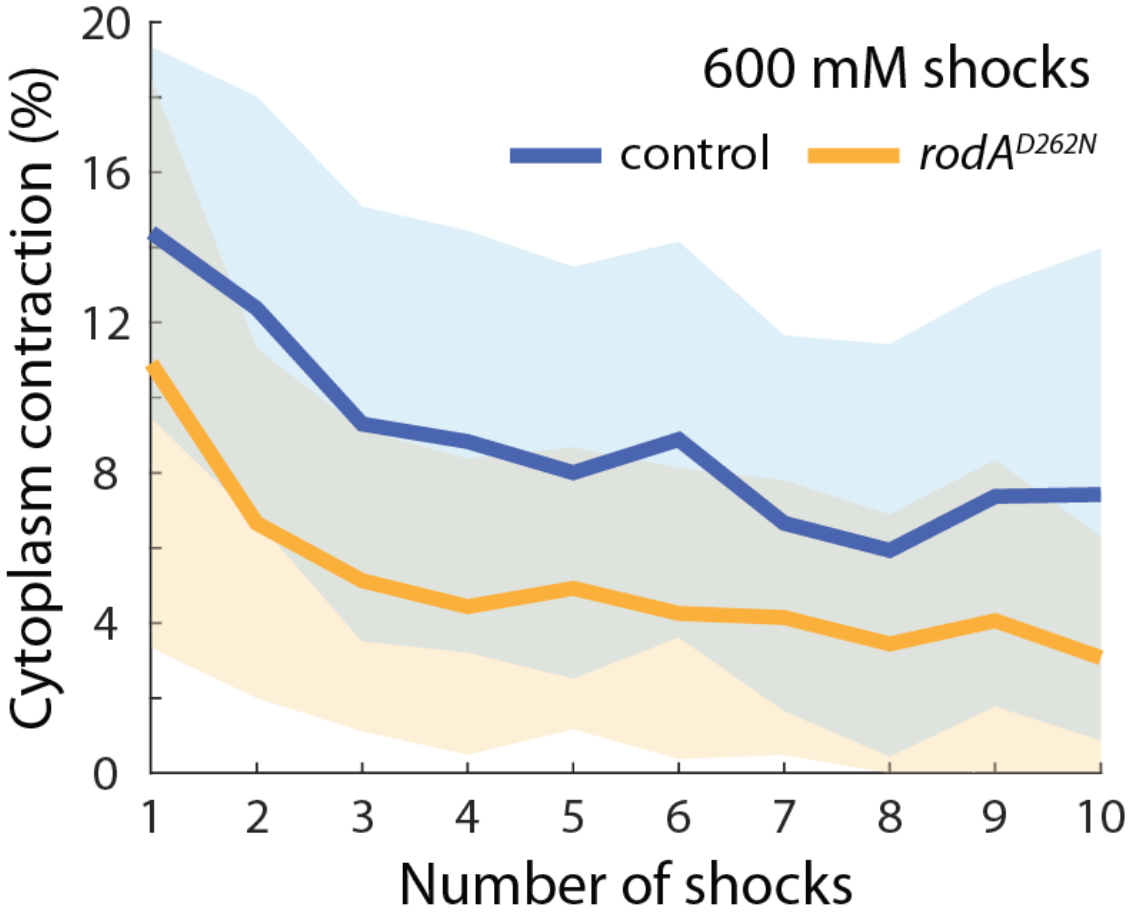

Figure S6: Overexpression of the dominant negative mutant *rodA*^{D262N} reduced cytoplasmic contraction during 600-mM osmotic shocks.

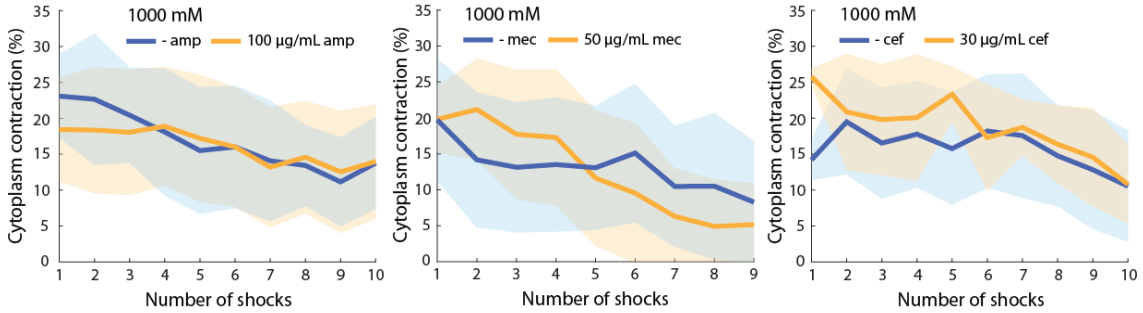

Figure S7: Inhibition of PBPs by 50 µg/mL mecillinam, 30 µg/mL cefsulodin, or 100 µg/mL ampicillin did not impact the dynamics of cytoplasmic contraction during 1-M shocks.

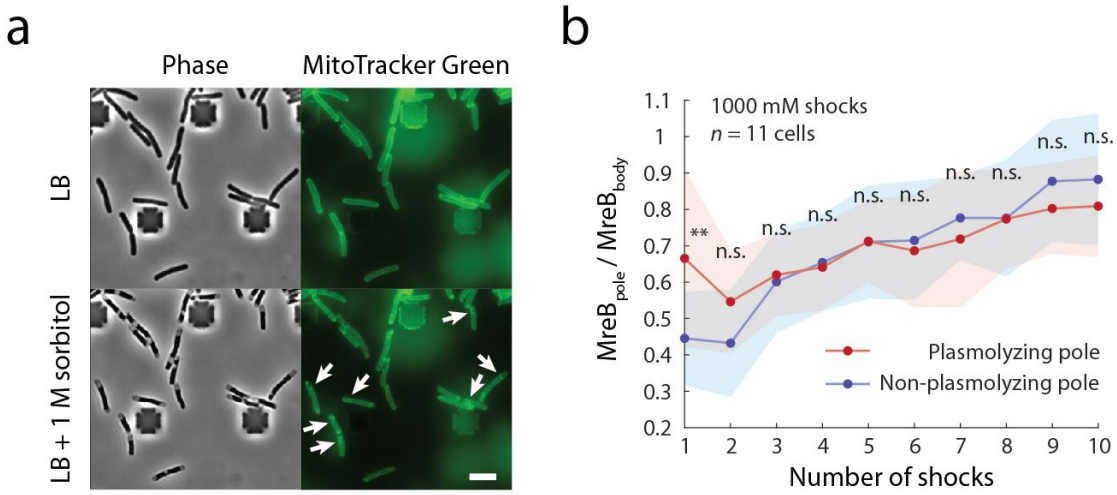

680

681 **Figure S8: MreB relocalization to each cell poles during hyperosmotic shocks**

682 **is not dependent on the magnitude of cytoplasmic contraction at the pole.**

683 a) Plasmolysis resulted in clear regions with negative mean curvature near

684 cell poles. The cytoplasmic membrane was stained with MitoTracker

685 Green. Scale bar: 5 μm.

686 b) During plasmolysis, many cells exhibited cytoplasmic contraction at only

687 one cell pole. No significant difference was observed between MreB

688 relocalization at the two poles after repeated shocks. Fluorescence was

689 evaluated during times of normal osmolarity to avoid bias caused by

690 plasmolysis. n=11 cells. **: $p < 0.01$, n.s.: $p > 0.01$; Welch's t-test was

691 performed for each osmotic shock cycle.

692 **Supplementary Table**

Strain	**Genotype**	**Source/reference**
MG1655	F^-, lambda$^-$, *rph-1*	CGSC #6300
KC1016	MG1655 pZS21-GFP	Gift from Thomas Silhavy
KC508	MG1655 *mreB-msfGFP*	[33]
KC496	MG1655 Δ*lacIZYA*::frt Δ*ponA*::frt attλ::pTB309(*Para*::*ponA*)	[55]
pPR1	MG1655 *Ptac*::*pbpA-rodA*^{D262N}	[35]
pPR6	MG1655 *Ptac*::*pbpA-rodA*	[35]
BW25113	F^- λ^- Δ(*araD-araB*)567 Δ*lacZ*4787(::*rrnB*-3) *rph-1* Δ(*rhaD-rhaB*)568 *hsdR514* pZS21-GFP	Gift from Jie Xiao
Δ*mltG*	BW25113 Δ*mltG*::*cmR* pZS21-GFP	This study
IMB1056	MC4100 *ara*^{R} *bamA*^{E470K} Δ*bamD*	[41]
IMB1144	IMB1056 *attHK*::*Plac-mCherry* pZS21-GFP	[41]
Plasmids	**Genotype**	**Source/reference**
pZS21-GFP	*pZS21kan::GFP*	Gift from Thomas Silhavy
pPR1	*Ptac*::*pbpA-rodA*^{D262N}	[35]

pPR6	*Ptac*::*pbpA-rodA*	[35]

693 **Table S1: *E. coli* strains and plasmids used in this study.**

694

695 **Supplemental Movies**

696

697 **Supplemental Movie 1: A22 treatment (100 μg/mL) depolymerizes MreB**

698 **filaments within 10 min in LB medium.** Scale bar: 5 μm.

Acknowledgements

The authors thank the Huang lab for helpful discussions. The authors acknowledge support from a Stanford Interdisciplinary Graduate Fellowship (to J.S.), NIH RM1 Award GM135102 (to K.C.H.), and NSF Award EF-2125383 (to K.C.H.). K.C.H. is a Chan Zuckerberg Biohub Investigator. This work was also supported in part by the National Science Foundation under Grant PHYS-1607611 and the hospitality of the Aspen Center for Physics.

706 **References**

707 1 Mitchell, A. M. & Silhavy, T. J. Envelope stress responses: balancing
708 damage repair and toxicity. *Nature Reviews Microbiology* **17**, 417-428 (2019).
709 2 Persat, A. *et al.* The mechanical world of bacteria. *Cell* **161**, 988-997 (2015).
710 3 Rojas, E. R. & Huang, K. C. Regulation of microbial growth by turgor
711 pressure. *Current Opinion in Microbiology* **42**, 62-70 (2018).
712 4 Deng, Y., Sun, M. & Shaevitz, J. W. Direct measurement of cell wall stress
713 stiffening and turgor pressure in live bacterial cells. *Physical review letters*
714 **107**, 158101 (2011).
715 5 Silhavy, T. J., Kahne, D. & Walker, S. The bacterial cell envelope. *Cold*
716 *Spring Harbor perspectives in biology* **2**, a000414 (2010).
717 6 Höltje, J.-V. Growth of the stress-bearing and shape-maintaining murein
718 sacculus of Escherichia coli. *Microbiology and molecular biology reviews* **62**,
719 181-203 (1998).
720 7 Rojas, E., Theriot, J. A. & Huang, K. C. Response of Escherichia coli
721 growth rate to osmotic shock. *Proceedings of the National Academy of*
722 *Sciences* **111**, 7807-7812 (2014).
723 8 Egan, A. J., Errington, J. & Vollmer, W. Regulation of peptidoglycan
724 synthesis and remodelling. *Nature Reviews Microbiology* **18**, 446-460 (2020).

725 9 Shi, H., Bratton, B. P., Gitai, Z. & Huang, K. C. How to build a bacterial
726 cell: MreB as the foreman of E. coli construction. *Cell* **172**, 1294-1305 (2018).
727 10 Sutterlin, H. A. *et al.* Disruption of lipid homeostasis in the Gram-negative
728 cell envelope activates a novel cell death pathway. *Proceedings of the*
729 *National Academy of Sciences* **113**, E1565-E1574 (2016).
730 11 Grimm, J. *et al.* The inner membrane protein YhdP modulates the rate of
731 anterograde phospholipid flow in Escherichia coli. *Proceedings of the*
732 *National Academy of Sciences* **117**, 26907-26914 (2020).
733 12 Sun, J., Rutherford, S. T., Silhavy, T. J. & Huang, K. C. Physical properties
734 of the bacterial outer membrane. *Nature Reviews Microbiology* **20**, 236-248
735 (2022).
736 13 Rojas, E. R. *et al.* The outer membrane is an essential load-bearing element
737 in Gram-negative bacteria. *Nature* **559**, 617-621 (2018).
738 14 Mathelié-Guinlet, M., Asmar, A. T., Collet, J.-F. & Dufrêne, Y. F.
739 Lipoprotein Lpp regulates the mechanical properties of the E. coli cell
740 envelope. *Nature communications* **11**, 1789 (2020).
741 15 Park, J. S. *et al.* Mechanism of anchoring of OmpA protein to the cell wall
742 peptidoglycan of the gram-negative bacterial outer membrane. *The FASEB*
743 *Journal* **26**, 219 (2012).

744 16 Sandoz, K. M. *et al.* β-Barrel proteins tether the outer membrane in many
745 Gram-negative bacteria. *Nature microbiology* **6**, 19-26 (2021).
746 17 Deghelt, M. *et al.* Peptidoglycan–outer membrane attachment generates
747 periplasmic pressure to prevent lysis in Gram-negative bacteria. *Nature*
748 *Microbiology*, 1-12 (2025).
749 18 Haswell, E. S., Phillips, R. & Rees, D. C. Mechanosensitive channels: what
750 can they do and how do they do it? *Structure* **19**, 1356-1369 (2011).
751 19 Auer, G. K. *et al.* Mechanical genomics identifies diverse modulators of
752 bacterial cell stiffness. *Cell systems* **2**, 402-411 (2016).
753 20 Wang, S., Arellano-Santoyo, H., Combs, P. A. & Shaevitz, J. W. Actin-like
754 cytoskeleton filaments contribute to cell mechanics in bacteria. *Proceedings*
755 *of the National Academy of Sciences* **107**, 9182-9185 (2010).
756 21 Fletcher, D. A. & Mullins, R. D. Cell mechanics and the cytoskeleton.
757 *Nature* **463**, 485-492 (2010).
758 22 Liu, X., Biboy, J., Consoli, E., Vollmer, W. & den Blaauwen, T. MreC and
759 MreD balance the interaction between the elongasome proteins PBP2 and
760 RodA. *PLoS Genetics* **16**, e1009276 (2020).
761 23 Shiomi, D. *et al.* Mutations in cell elongation genes mreB, mrdA and mrdB
762 suppress the shape defect of RodZ‐deficient cells. *Molecular microbiology*
763 **87**, 1029-1044 (2013).

764 24 Colavin, A., Shi, H. & Huang, K. C. RodZ modulates geometric
765 localization of the bacterial actin MreB to regulate cell shape. *Nature*
766 *communications* **9**, 1280 (2018).
767 25 Garner, E. C. *et al.* Coupled, circumferential motions of the cell wall
768 synthesis machinery and MreB filaments in B. subtilis. *Science* **333**, 222-225
769 (2011).
770 26 Domínguez-Escobar, J. *et al.* Processive movement of MreB-associated cell
771 wall biosynthetic complexes in bacteria. *Science* **333**, 225-228 (2011).
772 27 Van Teeffelen, S. *et al.* The bacterial actin MreB rotates, and rotation
773 depends on cell-wall assembly. *Proceedings of the National Academy of*
774 *Sciences* **108**, 15822-15827 (2011).
775 28 Lee, T. K. *et al.* A dynamically assembled cell wall synthesis machinery
776 buffers cell growth. *Proceedings of the National Academy of Sciences* **111**,
777 4554-4559 (2014).
778 29 Garner, E. C. Toward a mechanistic understanding of bacterial rod shape
779 formation and regulation. *Annual Review of Cell and Developmental Biology*
780 **37**, 1-21 (2021).
781 30 Sun, J., Shi, H. & Huang, K. C. Hyperosmotic Shock Transiently
782 Accelerates Constriction Rate in Escherichia coli. *Frontiers in Microbiology*
783 **12**, 718600 (2021).

784 31 Eberhardt, C., Kuerschner, L. & Weiss, D. S. Probing the catalytic activity
785 of a cell division-specific transpeptidase in vivo with β-lactams. *Journal of*
786 *bacteriology* **185**, 3726-3734 (2003).
787 32 Ouzounov, N. *et al.* MreB orientation correlates with cell diameter in
788 *Escherichia coli*. *Biophysical Journal* **111**, 1035-1043 (2016).
789 33 Ursell, T. S. *et al.* Rod-like bacterial shape is maintained by feedback
790 between cell curvature and cytoskeletal localization. *Proceedings of the*
791 *National Academy of Sciences* **111**, E1025-E1034 (2014).
792 34 Kuru, E. *et al.* In situ probing of newly synthesized peptidoglycan in live
793 bacteria with fluorescent D‐amino acids. *Angewandte Chemie International*
794 *Edition* **51**, 12519-12523 (2012).
795 35 Cho, H. *et al.* Bacterial cell wall biogenesis is mediated by SEDS and PBP
796 polymerase families functioning semi-autonomously. *Nature microbiology*
797 **1**, 1-8 (2016).
798 36 Yunck, R., Cho, H. & Bernhardt, T. G. Identification of MltG as a potential
799 terminase for peptidoglycan polymerization in bacteria. *Molecular*
800 *microbiology* **99**, 700-718 (2016).
801 37 Bohrhunter, J. L., Rohs, P. D., Torres, G., Yunck, R. & Bernhardt, T. G.
802 MltG activity antagonizes cell wall synthesis by both types of

803 peptidoglycan polymerases in Escherichia coli. *Molecular Microbiology* **115**,
804 1170-1180 (2021).
805 38 Bloom, M., Evans, E. & Mouritsen, O. G. Physical properties of the fluid
806 lipid-bilayer component of cell membranes: a perspective. *Quarterly*
807 *reviews of biophysics* **24**, 293-397 (1991).
808 39 Hwang, H., Paracini, N., Parks, J. M., Lakey, J. H. & Gumbart, J. C.
809 Distribution of mechanical stress in the Escherichia coli cell envelope.
810 *Biochimica et Biophysica Acta (BBA)-Biomembranes* **1860**, 2566-2575 (2018).
811 40 Ranjit, D. K. & Young, K. D. The Rcs stress response and accessory
812 envelope proteins are required for de novo generation of cell shape in
813 Escherichia coli. *Journal of bacteriology* **195**, 2452-2462 (2013).
814 41 Mikheyeva, I. V., Sun, J., Huang, K. C. & Silhavy, T. J. Mechanism of outer
815 membrane destabilization by global reduction of protein content. *Nature*
816 *communications* **14**, 5715 (2023).
817 42 Bratton, B. P., Shaevitz, J. W., Gitai, Z. & Morgenstein, R. M. MreB
818 polymers and curvature localization are enhanced by RodZ and predict E.
819 coli's cylindrical uniformity. *Nature communications* **9**, 2797 (2018).
820 43 Vadia, S. *et al.* Fatty acid availability sets cell envelope capacity and
821 dictates microbial cell size. *Current Biology* **27**, 1757-1767. e1755 (2017).

822 44 Shi, H. *et al.* Starvation induces shrinkage of the bacterial cytoplasm.
823 *Proceedings of the National Academy of Sciences* **118**, e2104686118 (2021).
824 45 Wong, F., Garner, E. C. & Amir, A. Mechanics and dynamics of
825 translocating MreB filaments on curved membranes. *Elife* **8**, e40472 (2019).
826 46 Miller, S. I. & Salama, N. R. The gram-negative bacterial periplasm: Size
827 matters. *PLoS biology* **16**, e2004935 (2018).
828 47 Miguel, A. *et al.* Modulation of bacterial cell size and growth rate via
829 activation of a cell envelope stress response. *bioRxiv*, 2022.2007.
830 2026.501648 (2022).
831 48 Zietek, M. *et al.* Bacterial cell widening alters periplasmic size and
832 activates envelope stress responses. *BioRxiv*, 2022.2007. 2026.501644 (2022).
833 49 Al-Mosleh, S., Gopinathan, A., Santangelo, C. D., Huang, K. C. & Rojas, E.
834 R. Feedback linking cell envelope stiffness, curvature, and synthesis
835 enables robust rod-shaped bacterial growth. *Proceedings of the National*
836 *Academy of Sciences* **119**, e2200728119 (2022).
837 50 Baba, T. *et al.* Construction of Escherichia coli K‐12 in‐frame, single‐
838 gene knockout mutants: the Keio collection. *Molecular systems biology* **2**,
839 2006.0008 (2006).
840 51 Edelstein, A. D. *et al.* Advanced methods of microscope control using
841 μManager software. *Journal of biological methods* **1**, e10 (2014).

842 52 Ursell, T. *et al.* Rapid, precise quantification of bacterial cellular
843 dimensions across a genomic-scale knockout library. *BMC biology* **15**, 1-15
844 (2017).
845 53 Sliusarenko, O., Heinritz, J., Emonet, T. & Jacobs‐Wagner, C. High‐
846 throughput, subpixel precision analysis of bacterial morphogenesis and
847 intracellular spatio‐temporal dynamics. *Molecular microbiology* **80**, 612-
848 627 (2011).
849 54 Shi, H. *et al.* Deep Phenotypic Mapping of Bacterial Cytoskeletal Mutants
850 Reveals Physiological Robustness to Cell Size. *Curr Biol* **27**, 3419-3429
851 e3414 (2017). https://doi.org:10.1016/j.cub.2017.09.065
852 55 Paradis-Bleau, C. *et al.* Lipoprotein cofactors located in the outer
853 membrane activate bacterial cell wall polymerases. *Cell* **143**, 1110-1120
854 (2010).

855